



Original Research Article

An overview on recent trends of spinel ferrites (MFe_2O_4 : $M = Fe^{2+}, Co^{2+}, Mn^{2+}, Ni^{2+}, Zn^{2+}$) synthesis and catalytic applications

^{1*} Vidya Singh

^{1*} Department of Chemistry, Maharana Pratap Govt. P. G. College, Hardoi-241001, U.P, India

Received: 2024-09-20

Accepted: 2024-12-06

Published: 2024-12-07

ABSTRACT

The synthesis of efficient catalysts is a key strategy for addressing the environmental and energy problems. Catalytic research has focused a lot of interest on spinel ferrites, which have a chemical formula of MFe_2O_4 ($M = Fe^{2+}, Co^{2+}, Mn^{2+}, Ni^{2+}, Zn^{2+}$ etc). A multitude of surface-active sites, high catalytic activity and ease of modification are only a few of the many physicochemical characteristics of spinel ferrites, which are caused by the metal cations changeable location and valence flexibility. Meanwhile, their special benefits in recycling and regeneration because of their magnetic characteristics promote their practical use potential. This article examines how spinel ferrites are made utilizing conventional and environmentally friendly chemical processes. Most significantly, a thorough review of the major pathways, mostly connected to selective doping, site replacement, structural reversal, defect introduction and linked composites is provided in order to enhance catalytic performance. A review is also given to the many catalytic uses of spinel ferrites and the composites they produce, such as Fenton-type catalysis, photocatalysis, electrocatalysis, and photo-electro-chemical catalysis. Important factors including recovery, reuse, and toxicity are also addressed. It is anticipated that spinel ferrites will be utilized in energy and environmental applications in the future. These applications will be driven by the development of expert modification, accurate synthesis, complex characterisation, and theoretical calculations.

Keywords: Applications, Dopants, Transition metal, Spinel Ferrites, Synthesis

*Corresponding author email address: vidyasingh005@gmail.com

Introduction

The world environment has seen unparalleled devastation in recent decades due to the fast rise of industrialization and the provision of renewable energy has encountered significant obstacles. Investigating cutting-edge catalytic technology can help provide ecologically friendly energy and address unsolvable environmental issues. These days, catalytic advanced technology is used in many facets of life, including biomedical treatment, renewable energy generation and environmental cleanup [1-4]. Since the components and structure have a major influence on the catalytic performance, it is imperative to build appropriate catalysts. Spinel ferrites are naturally occurring metal material catalysts with excellent catalytic efficiency, facile production, and easy recycling [5]. Because the catalytic activity may be adjusted by changing the cation's location and valence metal, it is also feasible to construct the ideal catalyst [6]. Due to spinel ferrites exceptional magnetic, biocompatible, and catalytic qualities, both scientists and the general public have shown interest in them thus far [7–10]. Divalent ions have the chemical formula MFe_2O_4 for spinel ferrites since they are also referred to as Fe^{2+} , Mg^{2+} , Co^{2+} , Ni^{2+} , Zn^{2+} and Mn^{2+} [11,12]. $ZnFe_2O_4$ is one kind of normal spinel, tetrahedral and octahedral sites are occupied, respectively, by M(II) and Fe (III) [13]. Smaller cations are more likely to locate at M sites, whereas bigger cations are more likely to locate at Fe (III) sites because octahedral sites often have wider interstices than tetrahedral sites [4]. Alternatively, with the aid of M(II), half of the Fe (III) locates octahedral sites (like $NiFe_2O_4$), while the other half finds tetrahedral sites with inverse spinel [14]. The tetrahedral and octahedral sites in complex spinel are randomly occupied by M(II) and Fe (III). $Mn_{0.8}Fe_{0.2}(Mn_{0.2}Fe_{1.8})O_4$ is one possible representation of $MnFe_2O_4$, which is formalized as complex spinel [15]. Three thousand years ago, magnet Fe_3O_4 was the first use of spinel ferrites, but no more research was done on the material for a very long period [16]. Nanomaterials have improved catalytic, thermal, mechanical, optical, and electrical performance when compared to large-sized materials [17-21]. In the meanwhile, spinel ferrites are useful due to their broad range of acid and alkaline adaptation [22]. The simplicity with which most spinel ferrites may be recycled with the use of an external magnet lends credence to green chemistry principles [23]. Nevertheless, the catalytic activity of pure spinel ferrites is restricted by limited electron mobility and low electrical conductivity.

As a result, a number of studies investigate excellent catalytical nanomaterials and strategies for improving them to control surface structure, agglomeration, particle size, morphology, and lattice integrity [24, 25]. Since the synthesis method has played a major role in performance improvement, previous research has mostly concentrated on environmental remediation, electrocatalysis, and synthetic methods [15, 26-27]. Relatively few studies have examined spinel ferrite modification strategies and their critical role in enhancing catalytic performance [4, 28]. The purpose of this review is to give a timely and motivational assessment for using spinel ferrites in catalytic applications appropriately. Eco-friendly techniques are presented along with common routes for spinel ferritin synthesis. Subsequently, a number of effective tactics are covered for enhancing overall catalytic performance: selective doping, site replacement, structural reversal, defect introduction, and linked composites. A brief explanation of the associated processes is included in the thorough presentation of the possible catalytic use in the environment and energy fields. Also covered are a few important points about toxicity. Last but not least, the final problems with spinel ferrites are suggested. Uniform nanoparticle synthesis is crucial since a nanoparticle's size greatly influence its electrical, optical, and magnetic characteristics. In general, the relative surface area of a nanoparticle increases with decreasing size. The two main methods used to create spinel ferrites are the green synthetic route and conventional synthesis. Two common methods for synthesis are the chemical and physical methods. Typically, Fe (III) and M(II) salts may be used as precursors to create spinel ferrites, and by varying the ratio and make-up of these salts, one can control the structural makeup of the final product. Biological methods are particularly acknowledged as green synthetic routes because of their favourable effects on the environment during the synthesis process and the biocompatibility of the final products. In the present review paper various method of synthesis of spinel ferrite, its application mainly photocatalytic, electrochemical application are explored.

Synthesis of Spinel Ferrites

The conventional example of the physical approach is the mechanical ball milling method, which is the oldest way to synthesis spinel ferrite. By using high-energy ball mills at high temperatures to create ultrafine powders from the combined compounds, contaminants can easily be introduced and the process takes a long time. In chemical synthesis, co-precipitation [29], hydrothermal synthesis [30], sol-gel auto-combustion route [31], and solid-state procedures [32] are

the most often used methods for creating spinel ferrites. Various methods of synthesis of spinel ferrite shown below in figure 1.

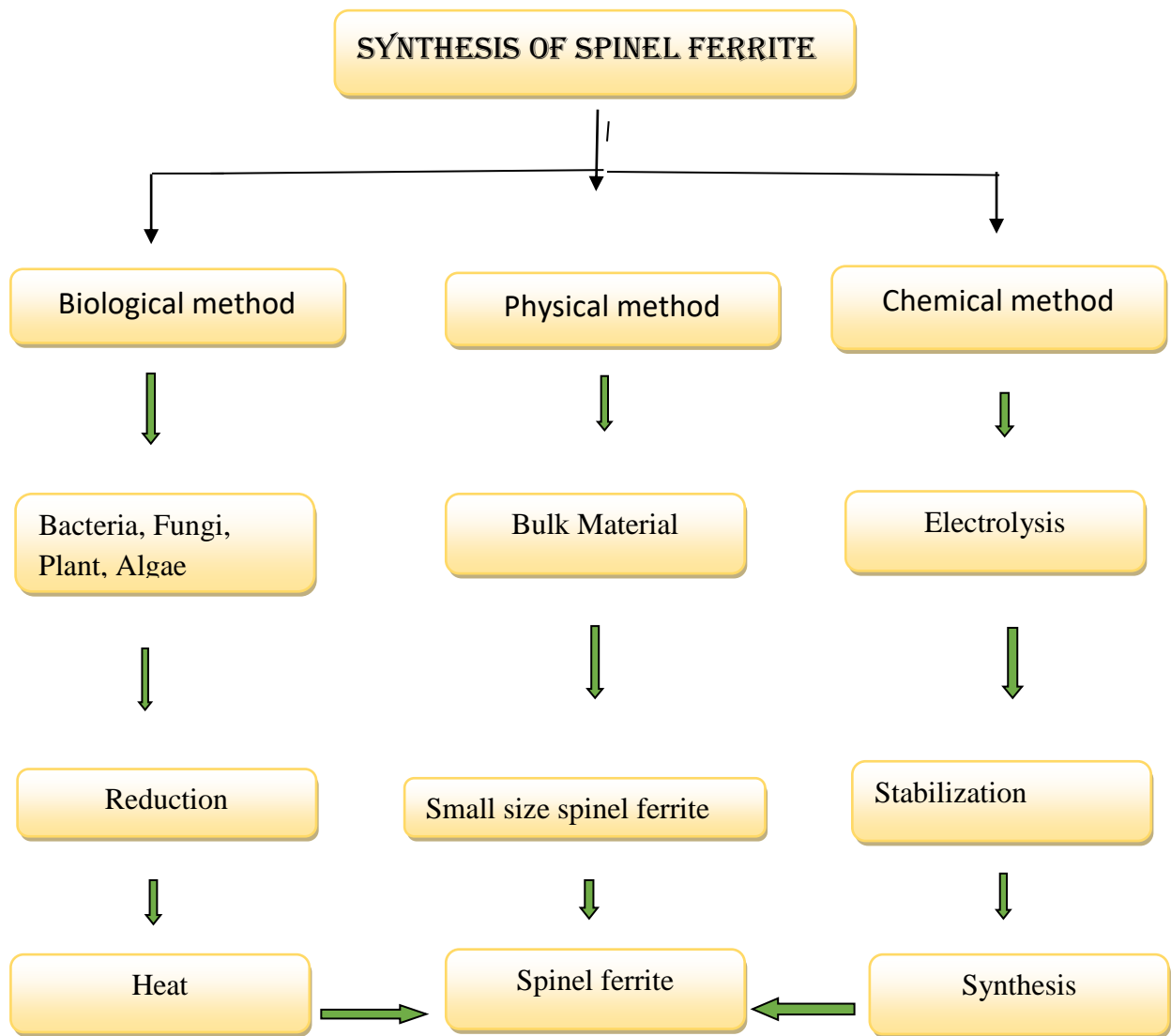


Fig.1. Synthesis of spinel ferrite

Co-precipitation method

A straightforward and affordable approach for making spinel ferrites is the co-precipitation process. Using a solution containing two or more different types of cations, one can achieve metal precipitation and get a precursor [32]. Precipitation and calcination can provide the desired substance. With the help of moderate conditions and the potential for direct synthesis in water,

this method has the potential to achieve large-scale preparation [33,34]. Co-precipitated CoFe_2O_4 nanoparticle's structure and magnetic properties were investigated in relation to different calcination temperatures (500 °C, 800 °C) [35].

The size and magnetic characteristics of the crystallites were found to be significantly influenced by both the reaction and calcination temperatures. The size of the crystallite grew with the calcination temperature. This was due to the fact that the crystal nucleus needed less activation energy at higher calcination temperatures. Similarly, spinel $\text{Mg}_{1-x}\text{Ni}_x\text{Fe}_2\text{O}_4$ ($x = 0.0, 0.6, 1.0$) nanoparticles were produced by Ajeesha et al. (2021) using the co-precipitation approach, and their structural, magnetic, optical, and photocatalytic capabilities were investigated [36]. According to crystal structure, there are three different forms of spinel's: complex, inverse, and normal shown below in figure 2 [12].

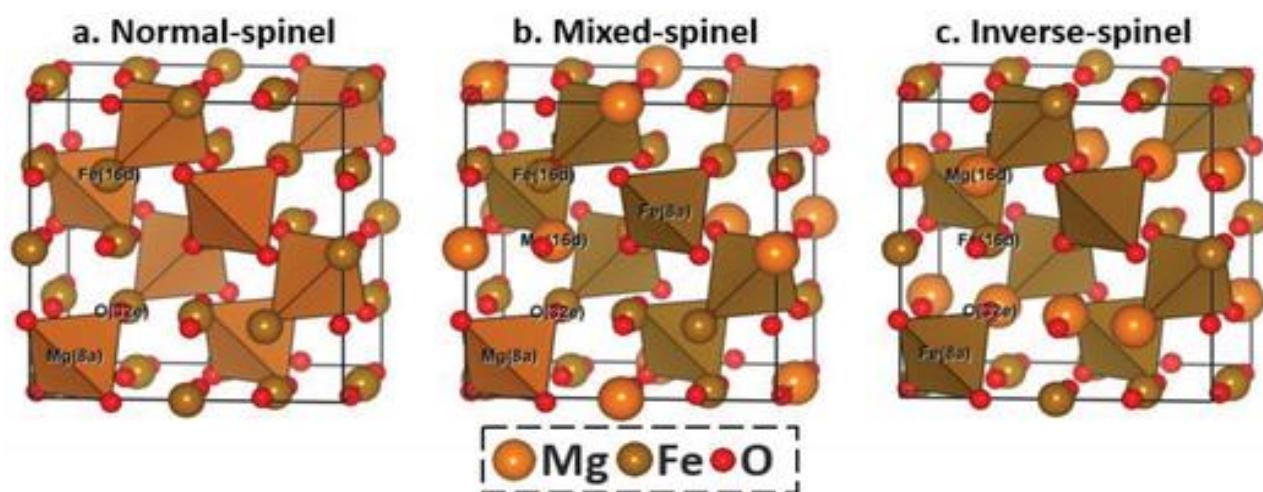


Fig. 2 Structures of a normal, inverse and complex spinel [12]

Hydrothermal method

In order to induce crystallization, the most often used technique, hydrothermal synthesis, uses water as a carrier and requires high pressure and high temperature in a closed system. High temperatures (100–300 °C) and pressures (1–30 MPa) would enable all ions operating as reactants in solution to gain substantial energy and speed up the process [37]. A particle's microstructure is influenced by temperature, heating rate, stirring rate, and reaction length. For

instance, ZnFe_2O_4 in a variety of morphologies was synthesized, and the photo-Fenton activity for dye degradation was assessed. A study of the arrangement of hollow microspheres, porous nanorods, nanoparticles, and nanoflowers came next. $\text{Ca}_x\text{Mg}_x\text{Ni}_{1-2x}\text{Fe}_2\text{O}_4$ ($x \leq 0.05$) nanoparticles with a spherical form were synthesized by hydrothermal technique and utilized for 4-nitrophenol catalytic reduction [38]. This method is useful for producing compounds that are simple to hydrolyse or oxidize but difficult to synthesis in water. As a result of their interactions with reactants, organic solvents with a large number of functional groups may be added to produce new products. Alcohol was used as a solvent in the solvothermal synthesis of $\text{Ni}_x\text{Fe}_{3-x}\text{O}_4/\text{Ni}$ composites [39].

Sol-gel auto-combustion method

The metal and iron precursors are added in the sol-gel auto-combustion approach in order to create a gel [30, 40]. The precursors comprise Fe (III) and M(II) salts, which are uniformly disseminated into water or ethanol while being vigorously stirred in an alkaline environment to create a gel-like substance. Subsequently, the gel is desiccated and burned at various temperatures within the range of 450 to 800 °C. Sol-gel auto-combustion method produces material with high purity and outstanding homogeneity, but the synthesis conditions are difficult to manage and the organics employed in the process can occasionally be hazardous. Ni and Co influences on OER performance were investigated by creating $\text{Ni}_x\text{Fe}_{3-x}\text{O}_4$ ($0 < x < 1$) by the use of the sol-gel auto-combustion technique [41]. Synthesis, characterization and biological activities of ZnCr_2O_4 shown below in figure 3. The reduced pore size distribution, electron conductivity, electrode electrolytic connections, restricted surface area, and charge transfer caused the OER performance to decline with Co replacement. Ni's lower valence state was stabilized by Fe as its octahedral oxidation progressed from +2 to +3/+4 during OER.

Additionally, ferrite copper was created using the sol-gel auto-combustion method at various calcination temperatures. This process resulted in the observation of the spinel change from cubic to tetragonal, which was caused by the contact with the CuO phase [30]. Fenton catalysis removes gallic acid, but its efficacy decreased as the calcination temperature rose. Additionally, the rate at which copper ions, which are a component of Fenton catalysis, leached decreased noticeably [42]

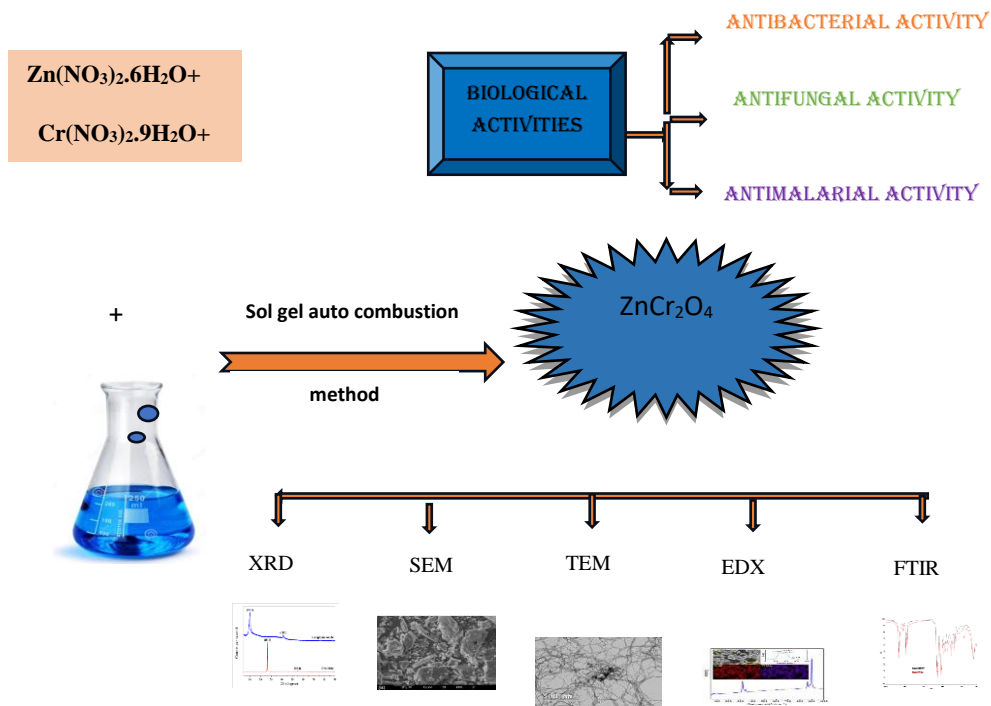


Fig. 3. Synthesis of $Zn_xCr_{3-x}O_4$ /Zn spinel oxides for different metal precursor ratios

In solid-state processes, iron and metal salts are ground to a powder at temperatures as high as as 1000°C. This mass-produced, cost-effective preparation is simple to use. One noteworthy aspect is the ability to create the material without the need for a solvent and the total avoidance of solvent-related contamination [43]. It is challenging to keep an eye on the operating procedure and choose the ideal circumstances for completing the reaction, nonetheless. Furthermore, separating the homogenous pure product from the reactant mixture is difficult. Various methods of synthesizing spinel $ZnFe_2O_4$ were examined for the purpose of producing hydrogen by photocatalysis produced by solar radiation. Among these techniques were the polymer complex (PC), microwave sintering (μW), solid-state reaction (SSR), and self-propagating combustion (SPC) approach [44]. These techniques produced crystals that were around 53 nm in size using the SSR method and 18 nm in size and a comparatively high surface area using the SPC approach. Apart from the techniques mentioned above, there are additional often employed artificial procedures, such the micro-emulsion method and the combustion method [45]. As conventional synthesis methods continue to be improved, new synthesis techniques are constantly being developed to achieve higher performance [46, 47]. For instance, $ZnFe_2O_4$ was

prepared via atomic layer deposition, and photochemical water oxidation performance was evaluated. A three-dimensional multilevel porous NiFeO spinel structure was created using a template sacrifice approach and super-assembly strategy [48, 49]. In order to offer stable polycrystalline structure and optimum electrical characteristics, the dominant octahedral filled spinel structure may be able to dominate the creation and breakdown of discharge products as well as effective active sites for complicated electrode processes. Furthermore, the NiFeO spinel's multistage pore structure successfully enhanced ion and material transport in addition to providing sufficient space for discharge products, significantly enhancing the positive electrode's catalytic performance.

Green chemistry and spinel ferrite (MFe₂O₄: M= Fe²⁺, Co²⁺, Mn²⁺, Ni²⁺, Zn²⁺)

Because of the high temperature and pressure support in the process, all of the aforementioned traditional ways to synthesis spinel ferrites typically demand substantial energy consumption. Furthermore, the use of some deadly substances and the limited technique may result in the appearance of toxic and dangerous by-products. Preparing spinel ferrites nano-materials via a green synthetic approach is notable since it follows sustainable routes. The primary focus of the spinel ferrites green synthesis pathway is waste utilization and biological methods. Magnetic nanoparticles are extracted from different bacteria using a biological technique. Bacteria may create magnetic spinel ferrites by a long-term mineralization process. For example, in figure 4 synthesis of spinel ferrite from biological resources and its characterization and applications explained [50]. Remarkably, surface-bound cell constituents and exopolysaccharides not only contributed to the creation of Fe₃O₄ nanorod shape but also to the production of PdAu alloy nanoparticles on the Fe₃O₄ nanorods. The reduction process of 4-nitrophenol and a few other nitroaromatic compounds could be catalysed by all three composites, although PdAu/Fe₃O₄ was shown to be the most effective. Due to the geometric and electrical consequences of Au's insertion, the Pd lattice contracted and the electron density decreased, improving the catalytic activity. [51] also produced that magnetic chitosan microspheres Fe₃O₄ @Ch-MNPs (CH = Chitosan; M = Au, Pd) by biomineralization with *Shewanella* algae. Chitosan prevented metal ions from corroding off MNPs and also acted as a transporter to modify the stable Au and Pd NPs on microspheres.

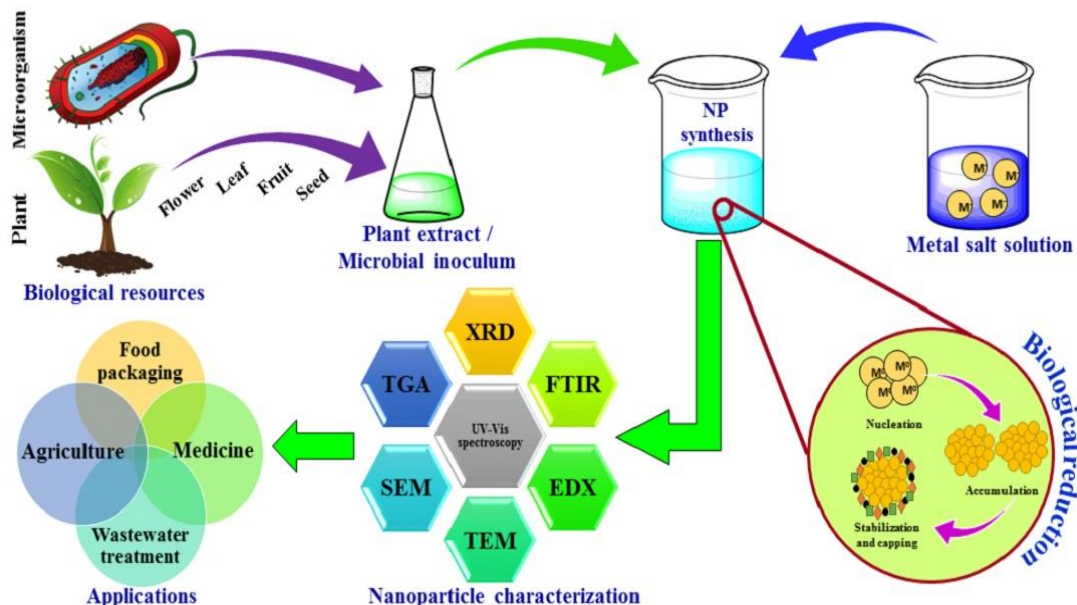


Fig. 4. Characterization and application of spinel ferrite synthesis from biological resources [50].

Furthermore, biological components from plants (e.g., seaweed, *Sesbania grandiflora* leaves, *Rubus glaucus* Benth, pineapple, watermelon, lemon juice, etc.) can be employed to assist in the formation of spinel ferrites by reducing metal ions into nanomaterials [52]. Among them are terpenoids, alkaloids, flavonoids, phenols, tannins, quinines, and other substances. The development of environmentally friendly processes is prompted by the significant roles that biomolecules play in particle formation and size/morphology control [53]. Plant extracts and metal salts are common reducing agents that can generate precursors. It is also possible to achieve the necessary structure, regulated morphology, and associated characteristics by varying a number of factors, including temperature, pH, reaction duration, metal salt concentration, and amount of reducing agent. NiFe_2O_4 was produced by Amiri et al. 2018 by using extract from the *Urtica* plant as a green precursor. The combination's active components were quinic acid and caffeic acid, which served as the capper and reducing agent, respectively [54]. In a similar manner, ZnFe_2O_4 (a reducing agent) was produced in *Limonia acidissima* juice. As a conclusion, 45 mL of deionized water and 5 mL of *Limonia acidissima* juice were mixed 1:2 with zinc and iron nitrates. The mixture was continuously stirred for 60 minutes, and it was then calcined for 4 hours at 600 °C [55]. In the meanwhile, it has been reported that the production of spinel ferrites involves the use of reducing agents such as coffee and *Glycyrrhiza glabra* [56]. Additionally, the

high energy consumption of conventional synthetic processes may be mitigated by using green fuel that is derived from inedible plant seeds to power the synthesis of spinel ferrites. Using the Jatropha-oil aided combustion approach, Ag-doped CuFe_2O_4 nanoparticles (ACNPs) were produced and exhibited remarkable (97%) photo-catalytic activity for Malachite green (MG) degradation, whereas host CuFe_2O_4 showed 87% [57]. The reduced arc radius's faster charge transfer rate may be the reason of the increased photocatalytic activity. In addition, a variety of metal-rich wastes, including old batteries and industrial waste residue, have been recycled to create spinel ferrites. Pretreatment and purification are the two steps that waste recovery typically involves. Following their crushing and screening, the resulting powders are purified even more before being leached in either nitric or sulfuric acid to extract the necessary metal. Using both actual and simulated electroplating wastewater, Huang et al. produced a variety of ferrites, with a metal ion recovery rate of greater than 98%. In order to decompose methylene blue (MB), CoFe_2O_4 -LIBs were created by extracting Co from wasted lithium-ion batteries [58].

In a similar manner, spinel ferrites MnFe_2O_4 -R (made using commercial reagents) and MnFe_2O_4 -B (manufactured using spent Zn- MnO_2 batteries) were generated [59]. These ferrites showed that the decolorization rate of MB was 98% and 92%. Studies have garnered a lot of interest because of spinel ferrites' significant potential in catalytic applications. In order to enhance catalytic performance, spinel ferrites are frequently doped with small-sized transition or rare earth metal ions to decrease the energy band gap. In the meanwhile, spinel ferrites' intrinsic drawbacks can be solved by combining them with other materials, and complimentary structural design can increase the application's reach. Consequently, a number of approaches are put forth, such as linked composites, selective doping, site replacement, structural reversal, and defect introduction.

Doping of transition metals (Fe^{2+} , Co^{2+} , Mn^{2+} , Ni^{2+} , Zn^{2+}) to Spinel ferrites

Spinel ferrites can be efficiently replaced with modest amounts of dopants to boost catalytic performance. When non-metallic or metallic elements are doped into spinel ferrites, the bandgap frequently experiences a red-shift transition and acceptor levels. In the valence band (VB) or conduction band (CB), the atomic orbitals of the dopant may hybridize with the narrow band, potentially yielding additional advantages such as improved carrier mobility and band gap

modulation. Selective doping can increase the material's electrical conductivity and promote electron migration. A useful auxiliary to trap electrons and stop electron-hole (e-h) pair recombination is also possible with the appropriate dopant. Elements that are used for doping include rare earth ions (La, Sm, Gd, Dy) and noble metals (Ag, Au, Pt, Pd).

Research on spinel ferrites doped non-metallically (usually with C, N, S, and P) has not advanced at the same rate as that of metal-doping methods. The surface structure and limited carrier mobility of spinel ferrites can be enhanced by doping metals. Additionally, the doped metals can function as active sites or electron traps in catalytic processes. Several metal-doped CaFe_2O_4 (CaFe_2O_4 ; M = Ag, Au, CuO, Pd, and Ir) were investigated in order to improve the photoreaction's low quantum efficiency [60]. CaFe_2O_4 crystal structure was further altered by doping other metals, although doping Ag metal strangely helped the distorted Fe core's crystal structure return to symmetry. In CaFe_2O_4 , O₂ 2p made up most of the VB while Fe 3d made up the majority of the minimal CB. The overlap between the O₂ 2p orbital and the Fe 3d orbital was critical to carrier movement. Because of the small and anisotropic three-dimensional orbits, reducing the symmetry around Fe greatly decreased the overlap. In light of this, Ag doping enhanced carrier mobility and strengthened the symmetry surrounding the Fe atom's core, both of which significantly boosted the photocurrent. Lattice distortion and lattice fringe configuration decreased as a result of the greater doping cation radius. Consequently, the values of the interplanar distance dropped from 2.51623 to 2.51570 Å, while the lattice parameter fell from 8.34538 to 8.34364 Å. As the copper doping ratio grew, the saturation magnetization in the Fe_3O_4 samples doped with copper ($\text{Cu}_x\text{Fe}_{1-x}\text{Fe}_2\text{O}_4$, x = 0, 0.2, 0.4, 0.6, 0.8, and 1.0) decreased. In contrast, the catalyst's catalytic effectiveness for breaking down methyl orange improved with time when NaBH_4 was present [61]. Mg doped CoFe_2O_4 was similarly reported by [62] as a photocatalyst for the degradation of rhodamine B (RhB). In the case of $\text{Co}_{0.6}\text{Mg}_{0.4}\text{Fe}_2\text{O}_4$ sample, where the Mg doping ratio was 0.4 weight percent, the highest photocatalytic degradation was 99.5%, 1.37 times more than that of pure CoFe_2O_4 (73%). Therefore, excellent charge separation and e-h pair recombination avoidance may be responsible for the enhanced photocatalytic performance. In contrast to metallic doping, non-metallic doping is more challenging to do as non-metallic elements are invariably present at the boundaries or gaps between atoms [63]. Doping spinel ferrites with non-metal elements

including sulphur, carbon, and nitrogen often increases catalytic performance because non-metal components can alter a crystal's band gap or electron mobility [17]. Since sulphur and oxygen have comparable chemical characteristics, sulphur may also be doped into CoFe_2O_4 . Sulphur doping of CoFe_2O_4 produced [64], sparse coral-like nanoparticles as opposed to pyknotic micro spherical ones. Moreover, a simple calcination procedure was used to create C/N doped CoFe_2O_4 in the air [65]. Higher carrier mobility and improved electron mobility between ions were made possible by the reduced intracellular distances caused by the lattice vibrations.

Site substitution

Spinel ferrite's octahedral or tetrahedral metal positions have a significant impact on its chemical and physical characteristics. These octahedral or tetrahedral position modifications often have an effect on architecture, thermal stability, and redox activity. Altering the octahedral location of Fe^{3+} to another metal would also modify the adsorption energy of $-\text{OH}$ at the catalytic sites and the metal-oxygen binding strength [66-68]. While rare earth ions (Ga, La, Sm, Gd, Dy) are frequently used to replace the Fe site, transition metals (Cu, Zn, Co, Ni, etc.) are typically used to replace the M site [69,70]. As for the M site, rare earth ions are frequently used to replace it.

Hence, the band gaps and flat band potential were controlled by Fe cations in the octahedral site but not in the tetrahedral sites [71]. It would also change the distribution of cations if Fe sites were substituted since Fe^{2+} autorotates electrons at the octahedral position. Therefore, controlling the amount of iron present in the octahedral sites may be able to achieve spinel's structural and electrical structure change. For example, solid state processes were used to create ZnFe_2O_4 , ZnFeGaO_4 , and ZnGa_2O_4 spinels. ZnFe_2O_4 and ZnFeGaO_4 were discovered to have a smaller band gap, which gives them poor activity under visible light irradiation. This is likely due to the electronic structural alteration caused by spin-polarized e_g and T_{2g} orbitals of Fe. In ZnGa_2O_4 , the band gap was dominated by the Ga 4s and O 2p orbitals with Ga replacement, whilst the broad dispersion of the Ga 4s orbitals ensures quick electron transmission in the conduction band. Due to Ga's occupancy of the octahedral sites, adding Ga to the ZnFe_2O_4 structure thus proven to increase light absorption in the UV area. In a similar manner, the $\text{Cu}^{2+}/\text{Cu}^+$ cation efficiently replaced the octahedral location of Fe_3O_4 , resulting in a larger specific surface area and strong segregation of Cu^{2+} and Cu^+ ions to the surface [72]. Additionally, during the co-precipitation

process that resulted in the production of spinel $\text{CuCr}_x\text{Fe}_{2-x}\text{O}_4$ ($0.0 < x \leq 1.0$) nanoparticles, quadrupole splitting and isomer translocations were caused by Cr^{3+} replacement, as shown by Mossbauer analysis. ($x = 0.00, 0.025, 0.050, 0.075, 0.10$) $\text{Co}_{0.30}\text{Cu}_{0.25}\text{Zn}_{0.45}\text{-Ce}_x\text{Fe}_{2-x}\text{O}_4$. Cu-Co-Zn ferrites replaced with cerium (Ce) were synthesized using the sol-gel auto-combustion process, and their structural, magnetic, morphological, and spectrum characteristics were examined.

The S-shaped M-H loops were observed to be changed when Ce was substituted in Cu-Co-Zn nano-ferrite, and this modification had a major effect on magnetism. This occurred as a result of cerium ions' larger radius than iron ions. In addition, the sample exhibited an aggregation form at higher Ce^{3+} concentrations and a cubic structure at lower Ce^{3+} values. The replacement of M sites in spinel ferrites with metal ions and the corresponding catalytic performance have been investigated. With M-site substitution, both the valance state and redox activity will shift. For instance, the surface of spinel ferrites may have an enrichment of Mn cations in +3 and +4 valence states [66]. In particular, the addition of Mn, but not Fe, to the catalyst's lattice boosted its oxygen content considerably. This enhanced the Mn and Fe^{3+} cations ability to oxidize on the catalyst's surface and promoted ferrite reduction. The $\text{CuFe}_2\text{O}_4 > \text{ZnFe}_2\text{O}_4 > \text{NiFe}_2\text{O}_4 > \text{CoFe}_2\text{O}_4$ degradation pathway was the one exhibited. Cu, Zn, Ni, and Co transition metal cations, were synthesized to substitute the M sites and alter the photo-Fenton activity for dye degradation [73]. According to the results of the magnetic investigation, Mn^{2+} might also take the place of Fe^{3+} in the octahedral position, reducing the super exchange contact and causing a drop in magnetism. Similarly, Ce-Dy substituted M-type barium hexaferrites' structural and optical characteristics were studied [68]. Grain size increased from 27.1 nm to 30.8 nm as a result of the replacement of Ce-Dy, which also led the secondary phase development of cubic CeO_2 and ortho DyFeO_3 .

Structure reversal of spinel ferrites

Although there is a lot of uncommon information available concerning spinel ferrites' structural reversal, production conditions, and mechanism, some new researches have shown us some unexpected results. The structural development of complicated spinel or inverse spinel can be caused by doping metal or non-metallic components. Because of its orbitals close to the Fermi level, the inverse spinel surface is more active than the standard spinel surface in terms of giving

or accepting electrons along the reaction route. Tatarchuk et al. (2017) doped ZnFe_2O_4 with Co to produce the anti-structure of CoFe_2O_4 [74]. For the first time, the zinc-cobalt ferrite system's antistructure modelling was taken into account, which may be utilized to change the structure and catalytic effectiveness of spinel ferrites. After structural reversal, octahedral Co was the donor and tetrahedral Fe was the acceptor in the lattice. An inverse spinel P- Fe_3O_4 with two active sites was also created on iron foam by phosphorus-doped modulation structure reversal [75]. It was discovered that phosphorus had no appreciable effect on P- Fe_3O_4 's electrical structure. As a result of the coordination between electrons and Fe ions becoming delocalized, P- Fe_3O_4 showed remarkable metallic and conductivity characteristics when its structure was reversed. As a result, Fe (II) and Fe (III) were able to quickly reverse in the octahedral state. Furthermore, compared to traditional spinel, the structure formed by partially replacing Fe atoms at the octahedral location with Co has been found to be more active (Fig 5).

Defect introduction:

A number of factors, related to catalysts, influence the pace of reaction; these include the number and quality of photo-induced e-h pairs that are produced, the surface migration and separation of the catalysts, and the interaction between the reactants and the e-h pairs [76]. Enhancing the e-h separation of semi-conductors has been demonstrated to be a successful use of defect engineering [77]. Meanwhile, additional active catalytic sites may be available due to the faulty states that have been produced [78]. For a long time, oxygen and cation vacancies have been the primary topics of the defect chemistry of spinel ferrites; in recent years, greater focus has been placed on the former [13]. According to recent research, adding defects at low concentrations can significantly change the electrical structure of metal oxide catalysts [79]. Evidence has demonstrated that flaws can serve as adsorption sites to reduce the rate of photo-excited electron transport, hence blocking recombination through the production of holes by photoexcitation. These results might provide a strong basis for the design of defects, their control, and the continued use of spinel ferrites. Above all, the generated oxygen defects have the ability to control the electron configuration, facilitating charge transfer. $\text{ZnFe}_{0.8}\text{Co}_{0.4}\text{O}_{2.4}$, for instance, is an oxygen-rich defect that was produced by cobalt doping and calcined in air for six hours at 600°C [80].

Moreover, amorphous N, P, and F tri-doped CoFe_2O_4 was doped with ionic liquid to introduce oxygen vacancies [81]. By securing ultra-fine MoS_2 nanoclusters to the surface, the specific surface area rose concurrently. Calculations using density functional theory (DFT) indicated that the lower inter-mediate energy barrier and the modified electronic structure were responsible for the enhanced OER performance. Recent publication of oxygen-rich defects CoFe_2O_4 nanoparticles for practical water electrolysis revealed the creation of oxygen vacancies by calcination under N_2 . When the CoFe_2O_4 produced by co-precipitation cooled properly, it was designated as CoF-1, CoF-2, and CoF-3. Afterwards, it underwent further calcination at 350, 550, and 650 °C. Thus, the proportion of oxygen defects in CoF-1, CoF-2, and CoF-3 was just 0.2%, despite the fact that their corresponding lattice parameters were 8.3762, 8.3889, and 8.4091 Å (2, 9 and 10%, respectively). The metal-oxygen bond's length as well as the metal ion's electrical surroundings were altered by these oxygen vacancies. Specifically, the oxygen vacancy-regulated CoFe_2O_4 may enhance the catalyst's intrinsic conductivity by restoring the neighbouring metal's orbit around the vacant negative ion site, thereby lowering the free energy of intermediate adsorption and making water electrolysis feasible.

In contrast to oxygen vacancies, cation vacancies are the subject of fewer reports. According to the theoretical computation, oxygen vacancies might be formed energetically in environments with low oxygen levels [82, 83]. Open air can result in the formation of cationic vacancies because the energy required to generate them is relatively low in oxygen-rich environments, particularly in the octahedral configuration. Through the use of the sol-gel auto-combustion technique, a defective $\text{Fe}_{3-\delta}\text{O}_4$ doped with high-valent Mo and V cations was built, and the effectiveness of the lithium-ion intercalation cathode was examined (Figure 5) [84]. Moreover, doping V^{5+} resulted in a considerable decrease in crystal size and a marginal alteration in lattice micro strain, whereas doping Mo^{6+} greatly decreased lattice micro strain with no effect on crystal size [85–89].

Because of the locations for lithium accommodation that the enriched cation vacancies provided, the electrochemical charge storage capacity improved. An analogous process may be utilized to produce cation vacancies in NiFe_2O_4 by mechanical milling and high-temperature heat treatment at 1000 °C; however, further heating led to the defect gradually disappearing [90-95]. As the degree of heat treatment rose, it was predicted that Fe^{3+} and Ni^{2+} cations would fill cation gaps.

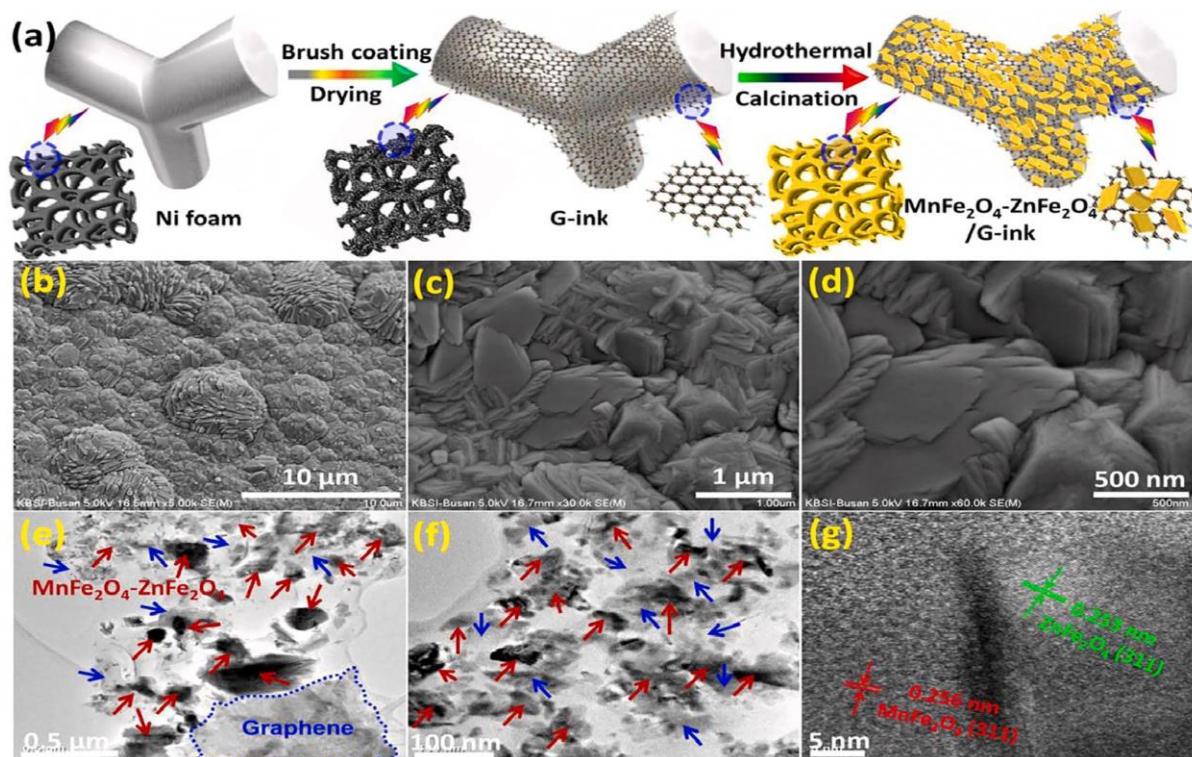


Fig.5 .(a) Fabrication for rhombus-like Mn-Zn-Fe-O/G-ink nanosheets on Ni foam surface. (b–d) SEM, (e, f) TEM and (g) HR-TEM images of rhombus-like Mn-Zn-Fe-O/G-ink nanosheets composite electrode

[84]

Catalytic application of spinel ferrites and their composites

Fenton-type catalysis

Fenton catalysis reaction potential is increased by the low cost of materials containing iron and the simple breakdown of hydrogen peroxide [96, 97]. Fenton-type catalysis has expanded beyond the original H_2O_2 activation to include permonosulfate (PMS), peroxydisulfate (PDS), and persulfate (PS) activations as a result of research advancements [98-101]. Table 1 presents spinel ferrites Fenton-type catalysis for pollutant degradation. A special set of benefits distinguish spinel ferrites catalysts from other materials. Divalent and trivalent ions can be present in the tetrahedral and octahedral interstices of spinel ferrites, respectively, allowing for the transformation of Fe^{3+} and Fe^{2+} in the Fenton reaction. MnFe_2O_4 , for instance, has been reported to remove norfloxacin (NOR) via H_2O_2 activation via sol-gel auto-combustion [40]. It was

confirmed that defluorination was the primary degradation process. Spinel ferrites, on the other hand, are able to effectively utilize the whole solar spectrum for the breakdown of poisons and pollutants due to their incredibly stable structure and tiny band gaps. Using a hydrothermal technique, Wang and associates created a novel ZIF-8-modified MnFe_2O_4 magnetic catalyst (ZIF = Zeolite imidazole framework). They found that for the breakdown of tetracycline (TC), 10% ZIF-8/ MnFe_2O_4 had higher photo-Fenton activity [102]. Two possible mechanisms for TC degradation in the 10% ZIF-8/ $\text{MnFe}_2\text{O}_4/\text{H}_2\text{O}_2/\text{vis}$ system were proposed. Visible light may activate MnFe_2O_4 under mechanism I, and the Zn-O-Fe structure may aid in the separation of e-h couples, Mechanism II: The Zn-O-Fe structure may have been inspired by MnFe_2O_4 , which might improve the separation efficiency of e-h couples. Although spinel ferrites are also capable of surpassing the acidity limit, the conventional Fenton technique requires an acidic reaction state (pH 2-4) [103].

Research findings indicated that spinel ferrites exhibited activity in the Fenton system throughout a pH range of neutral to basic. $\bullet\text{OH}$ may be produced from H_2O_2 by spinel ferrites such as MnFe_2O_4 , CuFe_2O_4 , CoFe_2O_4 , and Fe_3O_4 at pH = 4–8 [104]. It was suggested that there were two potential causes. Two observations were made: first, the pH of the TC solution affected the 10% ZIF-8/ MnFe_2O_4 adsorption capacity; second, the free radical's reaction pathway varied depending on the pH of the solution. Spinel ferrites are also readily recovered with an external magnetic field due to their scattered and ferromagnetic character. With relatively little Zn^{2+} and Fe^{3+} leaching, the orange II degradation rate in the $\text{ZnFe}_2\text{O}_4/\text{H}_2\text{O}_2$ system, for example, remained higher than 94% even after 5 cycles [31, 105]. The same was done for hierarchical ZnFe_2O_4 -600, which was easily isolated from the solution for the following cycle and had a saturation magnetization of 10.10 emu g^{-1} [106]. It is well established that spinel ferrites containing cobalt are active species capable of precipitating PMS. CoFe_2O_4 nanocrystals (CoFe_2O_4 NCs) were synthesized by combining PMS with bi-metal-organic frameworks (Co/Fe bi-MOFs) to form a well-defined porous structure that could degrade bisphenol A (BPA) [107]. Probably, the electrons were provided by Co (III) that climbed in octahedral sites. After receiving electrons at octahedral sites, Co (III) would change back to Co (II) in order to preserve the electron/charge balance on the surface of CoFe_2O_4 NC, indicating a redox cycle during PMS activation [108–111].

Table 1: Fenton type catalysis of cobalt spinel ferrites for pollutant degradation

Spinel ferrites	Pollutant	Pollutant Concentration	Catalysis dosage	Oxidation reagents	Activity	Ref.
CoFe/CoFe ₂ O ₄	Orange II	(60 mg/L)	0.05g/L	1.5 g/LPMS	96% Degradation (1 min.)	[28]
CoFe ₂ O ₄	Orange II	(20 mg/L)	0.05g/L	0.1 g/L Oxone	K=0.064 min ⁻¹	[31]
CoFe ₂ O ₄	MET	(10micro mol/L)	0.5g/L	2 mmol/L Na ₂ SO ₃	80.3% Degradation (40 min.)	[131]
CoFe ₂ O ₄	BPA	(50 mg/L)	0.1 g/L	0.45 mM PMS	K=0.112 min ⁻¹	[141]
Co _x Fe _{3-x} O ₄	BPA	(60 microM)	0.1 g/L	0.6 mM Oxone	97.6 % Degradation (60 min.)	[142]

Photocatalysis:

TiO₂ is the most widely used photocatalyst, as is widely known, although its poor capacity to absorb light in the ultraviolet (UV) spectrum makes it less useful [112]. The full solar spectrum may instead be absorbed by semiconductor metal oxides [113–115]. These characteristics set them apart from conventional semiconductor materials like TiO₂ (3.2 eV) and ZnO (3.2 eV). Improvements in chemical stability and photocatalytic performance are possible in the interim following alteration. For instance, it has been found that ZnFe₂O₄ nanocrystals may reduce Cr (VI) photo-catalytically without the need for further sacrificial reagents [116].

In the continuous mesoporous network with a large specific surface area, charge carriers might delocalize spatially [117]. Furthermore, a practical method for eliminating pollutants from the environment is to include PMS activation and photocatalysis into a system. When the ZnFe₂O₄/PMS system was used to accelerate the breakdown of Orange II, the clearance rate was about 100% in less than 80 minutes. The oxidation of absorbed water was the first step in the metal photoreduction process, and it was made feasible by holes or hydroxyl groups that were generated on the catalyst surface. Researchers have recently focused a great deal of emphasis on covering various metal oxides or carbon-based materials with spinel ferrites for photocatalysis.

To degrade BPA, a $\text{CoFe}_2\text{O}_4\text{-TiO}_2$ linked system was built shown below in figure 6 [118]. The combined $\text{CoFe}_2\text{O}_4/\text{PMS}$ system was mostly made up of $\text{SO}_4^{\bullet-}$ and $\bullet\text{OH}$, with significant reactivity and good reproducibility. Similarly, PS was intended to be induced for the breakdown of antibiotic pollutants, such as metronidazole, amoxicillin, tetracycline, and ciprofloxacin, using $g\text{-C}_3\text{N}_4/\text{MnFe}_2\text{O}_4/\text{graphene}$ ($\text{C}_3\text{N}_4@\text{MnFe}_2\text{O}_4\text{-G}$) nanocomposites.

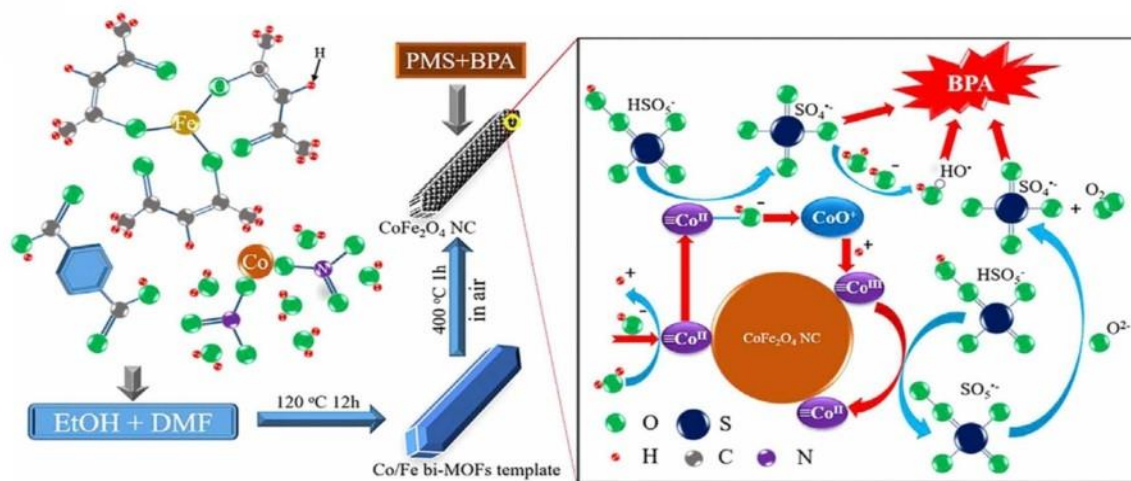


Fig. 6. Synthesis procedure for CoFe_2O_4 spinel ferrite and mechanism for BPA degradation by PMS activation [118]

The heterogeneous junction created by p-type CoFe_2O_4 and n-type TiO_2 interacted favourably with the redox reaction, facilitating charge transfer and lowering e-h pair recombination. Similarly, a $\text{CoFe}_2\text{O}_4@\text{CuS}$ heterojunction photocatalyst was developed to degrade penicillin G, with a maximum degradation of 70.7% shown in [119]. The production of h^+ , $\bullet\text{O}_2^-$, $\text{SO}_4^{\bullet-}$, and $\bullet\text{OH}$ was the reason for the metronidazole degradation of $\text{C}_3\text{N}_4@\text{MnFe}_2\text{O}_4\text{-G}$, which was 3.5 times that of pure $g\text{-C}_3\text{N}_4$. In the meanwhile, because of their huge surface area, low cost, simplicity of synthesis, and tiny band gaps, spinel ferrites have been preferred for photocatalytic hydrogen generation. The hydrogen generation sequence that was observed was $\text{NiFe}_2\text{O}_4/\text{mpg-CN} > \text{CoFe}_2\text{O}_4/\text{mpg-CN} > \text{MnFe}_2\text{O}_4/\text{mpg-CN} > \text{Fe}_3\text{O}_4/\text{mpg-CN} > \text{mpg-CN}$. The most hydrogen-yielding $\text{NiFe}_2\text{O}_4/\text{mpg-CN}$ was hypothesized to have a more pronounced concave form, which would increase the number of catalytic active sites for the hydrogen evolution process [120-121]. Additionally, photocatalytic CO_2 reduction using spinel ferrites has been studied. Formic acid, formaldehyde, methanol, ethane, methane, and carbon monoxide may all be produced from CO_2

[122]. By photo-catalytically reducing CO₂, hydrocarbon fuels are obtained that are safe for the environment to utilize as fuel feedstock. In summary, there are a few standard parameters for the reduction of CO₂, the production of H₂, and the degradation of contaminants by photocatalysis. CoAl₂O₄, MgFe₂O₄, and CoFe₂O₄ with small band gaps ($E_g < 1.55$ eV) were produced, with Na₂C₂O₄ acting as an electron donor, to synthesize formic acid under photocatalytic CO₂ reduction. The three requirements are a shift in the conduction band (CB) to a more negative area than the usual good charge separation [123], CO₂ reduction potentials [124], and small band gap for visible light absorption. Two factors may be used to summarize the main causes of the increased activity. The first was that because of the low redox potential, Na₂C₂O₄ may speed up the oxidation. The other was that Na₂C₂O₄ may increase the availability of carbon sources and encourage the production of formic acid [125-126]. By using a surfactant-assisted thermal technique, four distinct spinel ferrites (MFe₂O₄, M = Mn, Fe, Co, and Ni) were synthesized in a comprehensive manner. Particles on the surface of ZnFe₂O₄ enhanced light absorption and encouraged the separation of photo-induced e-h pairs [127-130].

Electrocatalysis

Because of its great element availability, low cost, environmental friendliness, and good performance, spinel material is acknowledged as an efficient noble-metal-free substitute. Mixed metal oxide compounds have been shown via studies to be promising candidates for electrocatalytic processes. Since spinel ferrites are bimetallic oxides, they have drawn a lot of interest in the field of electrocatalysis, particularly in relation to supercapacitors, oxygen evolution reaction (OER), and oxygen reduction reaction (ORR). Because of their coordination centre's tetrahedral/octahedral orientations and variety of metal oxidation states, spinel ferrites are advantageous for OER. In particular, the obtained MFe₂O₄ NFs material, which had an average diameter size of 150 nm and lengths that reached the dozens of micrometres, had exceptional surface areas and fractional porous structures, which were valuable to the mission path in terms of increased exposed catalytic active sites, decreased mass transfer resistance, and enhanced electrical conductivity. CoFe₂O₄ NFs > CuFe₂O₄ NFs > NiFe₂O₄ NFs > MnFe₂O₄ NFs > Fe₂O₃ NFs was the order in which the tested OER performance fell. A range of NiFe₂O₄ quantum dots (AT NiFe₂O₄ QDs) with atomic thinness demonstrated OER performance that was on par with commercial RuO₂ [78]. Two- and four-electron routes are common in the

complicated kinetics of ORR. The electrode surface initially adsorbs O_2 , which is subsequently reduced to H_2O or OH^- before being further reduced or disproportionated [131]. Similar outcomes were attained in the low-temperature efficient synthesis of four distinct 3D-rGO/iron oxide combinations (iron oxide = Fe_3O_4 , $\alpha-Fe_2O_3$, $\gamma-Fe_2O_3$, and $\alpha-FeOOH$) without sacrificing phase structure [132]. In an appropriately produced series of Mn-doped cobalt ferrite (MCF), the electrochemical activity displayed a "volcanic trend" as the manganese concentration increased [133].

These results offer useful guidance for the design of electrocatalysts as well as insight into the process of spinel ferritin electrocatalysis. Due to their strong OER and ORR activity, spinel ferrites have been referred to as bifunctional catalysts with a potential future in the development of metal-air batteries [134]. The hypothesis that combining hexafluoropropylene difluoride with a vinylidene difluoride separator might improve LiO_2 battery performance also spurred the notion to develop high-performance LiO_2 batteries by modifying the pore structure of electrocatalytic materials. Additionally, it demonstrated remarkable long-term cycle stability and rate capabilities. These artificial procedures might also be used to create three-dimensional carbonaceous nanomaterials, such metals or metal oxides, to maximize the use of advanced manufacturing in LIBs [135]. Co 3d electron delocalization and a change in spin state were brought about by Fe^{3+} ions entering the Co_3O_4 network. Fe^{3+} ions have the ability to successfully activate adjacent Co^{3+} ions by spin and charge action, which increases the inherent oxygen catalytic activity of Co_2FeO_4 . Additionally, research has demonstrated the potential use of spinel ferrites in super-capacitor energy storage systems. High energy, high power, and high-density supercapacitors that are lightweight and flexible are difficult to produce. Using a variety of oxidation state electrode materials with fast and reversible reactions is a useful technique to increase the energy density through the Faraday reaction, which will produce pseudo-capacitance. Hydrothermal hierarchical mesoporous $NiFe_2O_4$ nanoscale forest with super-high surface area was investigated. As a binder-free electrode, the $NiFe_2O_4$ nano cone forest growing on carbon cloth demonstrated a capacitance of 697 F g^{-1} at a scanning rate of 5 mV s^{-1} . Comparing electrochemical reduction to the energy-intensive and CO_2 releasing traditional Haber-Bosch processes, the latter method is less environmentally friendly and less sustainable for producing NH_3 . N_2 reduction reaction (NRR) was described by use of a spinel Fe_3O_4 nanorod

on a Ti mesh ($\text{Fe}_3\text{O}_4/\text{Ti}$). $\text{Fe}_3\text{O}_4/\text{Ti}$ generated NH_3 at a rate of up to $5.6 \times 10^{-11} \text{ mol s}^{-1} \text{ cm}^{-2}$ and 0.4 V, when compared to a reversible hydrogen electrode. That device has a 2.6% Faraday efficiency. Recent experiments have shown that ZnFe_2O_4 (ZFO), which is used as an electrode material in capacitive deionization, can desalinate ultra highly. ZFO capacitive deionization system based on nanoscale flake has the potential to desalinate up to 136.6 mg NaCl/g and operate steadily for 200 cycles of adsorption and desorption [136].

Photo electro-chemical catalysis:

In order to do water splitting using solar energy, photo electro-chemical cells, or PECs, are now a viable approach. A lot of attention has been paid to spinel ferrites that have the right band gap and abundance. The metal cation ferrites' rich valency, distinctive chemical makeup and selectivity are the sources of their strong photochemical catalytic activity. Modified conductivity and photoelectrode design can be achieved by utilizing distinct metal cations to drive electron migration and facilitate redox reactions. The voltage support needed for a photo electro-chemical (PEC) system is similar to that of commercial electrolyzes; however, in PEC systems, the optical voltage necessary for absorption of solar photons is the source of the required voltage. To facilitate the process of water splitting, photocatalysts must provide sufficient driving force to generate photovoltaic cells [137,138]. Under the Visible light irradiation photodegradation of bisphenol A by $\text{ZnFe}_2\text{O}_4\text{-TiO}_2$ shown below in figure 7.

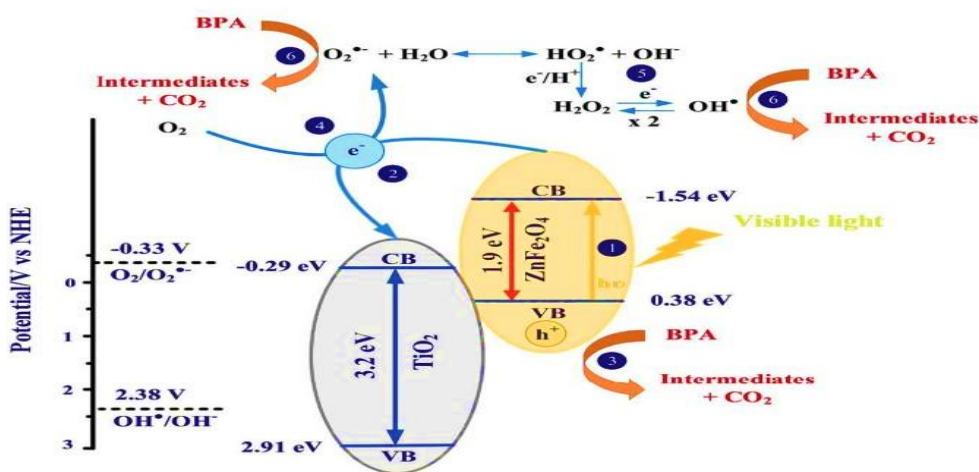


Fig. 7 .Visible light driven photodegradation of bisphenol A by $\text{ZnFe}_2\text{O}_4\text{-TiO}_2$ under visible light irradiation [137]

The ferrite electrode was first studied electrochemically in the 1970s. Several ferrites were explored after CdFe_2O_4 ferrite was originally used for PEC. These included $\text{Li}_{0.5}\text{Fe}_{2.5}\text{O}_4$, MgFe_2O_4 , Fe_3O_4 , p- CaFe_2O_4 , $\text{Ti}_x\text{Fe}_{3-x}\text{O}_4$, p- and n-type $\text{Co}_x\text{Fe}_{3-x}\text{O}_4$ and $\text{CoTi}_x\text{Fe}_{2-x}\text{O}_4$, p- CoFe_2O_4 , p- and n-type NiFe_2O_4 , n- ZnFe_2O_4 , and $\text{Zn}_x\text{Ti}_y\text{Fe}_{3-x-y}\text{O}_4$. Despite the relatively low reported efficiency of photocurrent, the early research focused only on the fundamental features of PECs and neglected to examine the internal process [139]. The process is strongly correlated with pH: in an acidic environment, proton reduction to H_2 is largely seen, whereas in an alkaline environment, water is mostly converted to hydroxide ions. Notably, because of its instability in an acidic environment, spinel ferrites' PEC reaction is favourable to neutral or alkaline solutions. Additionally, selective doping is a useful way to improve the subpar carrier transport ability. Spray pyrolysis, for instance, may be used to create a ZnFe_2O_4 photoanode doped with Ti^{4+} , wherein a little portion of the Fe^{3+} in the lattice is swapped out for Ti^{4+} [140,141]. 875 times the solar splitting photocurrent of the pure ZnFe_2O_4 photoanode was demonstrated by the Ti^{4+} doped ZnFe_2O_4 photoanode, which measured 0.35 mA cm^{-2} vs RHE at 1.23 V. Annealing and overlayer passivation are more methods for modifying the PEC performance of zinc ferrite nanorods.

After ZnFe_2O_4 was surface passivated with Al_2O_3 , the carrier density increased to $18.83 \times 10^{20} \text{ cm}^{-3}$ from $8.43 \times 10^{20} \text{ cm}^{-3}$ [142]. It was possible to prevent reverse electron transfer and charge recombination by minimizing surface imperfections using cover passivation, which led to the increase. Furthermore, ZnFe_2O_4 containing a lot of oxygen vacancies ($\text{Zn}_{1-x}\text{Fe}_x\text{Fe}_2\text{O}_{4-y}$) was effectively prepared by hydrogen reduction using self-doping Fe^{3+} [143]. As compared to pure ZnFe_2O_4 , the photocurrent density at 1.23 V versus RHE was 11. times higher at 0.22 mA cm^{-2} . Electrolyte interface charge transfer is facilitated by oxygen vacancies, which also improve electrical conductivity and speed up the kinetics of water oxidation. Fe^{3+} self-doping is advantageous for increasing carrier density. Many more investigations into the photoelectrochemical characteristics of various spinel ferrites have emerged in the interim. CuFe_2O_4 , MgFe_2O_4 , and ZnFe_2O_4 are three exemplary spinel ferrites whose nanostructured films were studied in order to evaluate their PEC characteristics [144]. The inherent n-type response was shown to be successfully improved by annealing treatment in conjunction with NiFeO_x (NFO) overlayers coating. An optical voltage of around 300 mV was restricted by a surface state of 0.9 V vs. RHE in all of the investigated spinel ferrites, resulting in substantial Fermi level pinning.

Surface conditions were not remitted; rather, the improved performance brought about by NFO coatings was due to the kinetics of water oxidation.

Toxicity, recovery and reuse:

The intrinsic toxicity of spinel ferrites cannot be disregarded, even with their great catalytic potential. The environment may thus be particularly vulnerable to the nano-sized spinels and their unavoidable metal ion leakage [145]. Apoptosis, downregulated metabolism, delayed hatching, tail/spinal cord curvature, and severe cardiac edema are among the acute negative effects of CoFe_2O_4 nanomaterials on zebrafish embryos [146]. Additionally, the agglomeration of nanomaterials and the leaching of metal ions (Co^{2+} and Fe^{3+}) caused severe mechanical damage and oxidative stress. Based on some research [147,148], there is less co-ion leakage, which may explain why CoFe_2O_4 is expected to be harmful both in vivo and in vitro. Before spinel ferrites are commercialized or used extensively, further research is required because opinions on their hazardous effects are divided. This is particularly true for the spinel ferrites that have been synthesized recently, which will probably be used in the future. Constructing ecologically safe spinels is crucial since the majority of ferrite nanoparticles have uncertain and debated negative implications. The examination of biocompatibility, which also looked at the non-toxicity of Fe_3O_4 /graphene NCs in live mice, confirmed that they are not cytotoxic [149]. Manganese spinel ferrites are safe for marine systems; a recent ecotoxicological assessment of *Mytilus galloprovincialis* mended with manganese spinel ferrites nanomaterials was carried out by Coppola et al. [150]. By combining with other substances, the toxicity of the nano-sized SFs can be decreased or completely removed in the interim. By assessing haematological parameters, white blood cells, and total enzyme activity, for instance, CoFe_2O_4 @sugar (table sugar) nanoparticles did not show any discernible harm on rats [151]. Indeed, nanomaterials have a high catalytic activity and a superior load capacity due to their huge surface area and tiny size. Unfortunately, it is challenging to remove nanomaterials from the medium efficiently due to their minuscule size. The two most common recycling methods for recovering spent catalysts are centrifugation and filtering [152], although these processes are time-consuming and expensive. Magnetically recovering spinel ferrites nanoparticles is a more efficient, selective, and cost-effective way than typical centrifugation and filtering techniques. All it takes is a basic external magnetic field. Magnetic spinel ferrites can therefore be used as a catalyst to speed up the

reaction process and address the majority of catalysts' recovery issues. According to research, most magnetic catalysts have recovery rates of more than 90%, and in some cases even up to 99%, which essentially satisfies industrial standards. The recovery of the catalyst is specifically impacted by the reaction circumstances, preparation techniques, magnetic strength, and kind of magnetic catalyst.

Therefore, creating the best possible preparation conditions is essential to synthesizing evenly dispersed magnetic catalysts. Active group coverage, metal ion leaching, and catalyst structural instability are linked to decreases in catalytic performance [153]. To hydrogenate cyclohexanone, 1,3 dinitro, and 4-nitroaniline, CoFe_2O_4 -APTES-Pd nanocomposites were created. They were effortlessly removed from the mixture by magnetic bar throughout the course of at least ten recycling cycles. The nanocomposites were provided with structurally stable catalytic sites by 3-ami-nopropyltriethoxysilane (3-APTES) and CoFe_2O_4 . The high hydrogen storage density of 62.47 g L^{-1} that $\text{Co}_{0.25}\text{Fe}_{2.75}\text{O}_4$ has, as shown by Li et al., indicates that it can hold onto hydrogen for over ten cycles. This really is amazing. On the other hand, research [108] discovered that $\text{Co}_{1.51}\text{Fe}_{1.49}\text{O}_4$ MDC's catalytic ability drastically decreased following the first cycle, reaching as low as 61% in the second. The catalyst's catalytic activity may be effectively restored by calcining it outdoors at $450 \text{ }^\circ\text{C}$.

Conclusion

Spinel ferrites have become a ubiquitous presence in modern life, particularly in the areas of biomedicine, communication, and catalysis. This research analyses several spinel ferrites production methods, including green synthesis and conventional chemical synthesis, based on their structure. Notably, prior research has focused primarily on-site substitution, defect introduction, selective doping, coupled composites, structure reversal, and modification strategies. This has sparked an imaginative conversation about these strategies, which can assist maximize spinel ferrites for enhanced catalytic efficacy. The catalytic uses of CoFe_2O_4 , CuFe_2O_4 , NiFe_2O_4 , and ZnFe_2O_4 seem to have a bright future with applications in Fenton-type catalysis, photocatalysis, electrocatalysis, ZnFe_2O_4 , Fe_3O_4 , and other mixed metal oxides. Finally, it is projected that spinel ferrites will be important catalysts for the breakdown of contaminants and water splitting, as well as for the widespread use of electrodes and

supercapacitors as energy storage devices. Although there has been a lot of improvement, more effort has to be done in order to achieve even greater advancement.

References:

- [1] H Wang, T Chen, D Chen, X Zou, M Li, F Huang, *Appl. Catal. B Environ.* 260, 118203 (2020).
- [2] M Aksoy, G Yanalak, E Aslan, İH Patır, M Önder, *Int. J. Hydrog. Energy*, 45,16509 (2020).
- [3] Y Alsalka, LI Granone, W Ramadan, A Hakki, R Dillert, *Appl. Catal. B Environ*, 244,1065 (2019).
- [4] S Chandrasekaran, C Bowen, P Zhang, Z Li, Q Yuan, X Ren, *J. Mater. Chem. A* 6,11078 (2018).
- [5] M Amiri, K Eskandari, M Salavati-niasari, *Adv. Colloid Interf. Sci.*, 271, 101982 (2019).
- [6] Y Yang, Y Xiong, ME Holtz, X Feng, R Zeng, G Chen, *Proc. Natl. Acad. Sci.*116, 24425 (2019).
- [7] Y Du, W Ma, P Liu, B Zou, J Ma, *J. Hazard. Mater.*308, 58 (2016).
- [8] M Madhukara Naik, HS Bhojya Naik, G Nagaraju, M Vinuth, H Raja Naika, K Vinu, *Microchem. J.*,146,1227(2019).
- [9] P Samoila, C Cojocaru, L Sacarescu, P Pascariu, A Domocos, A Rotaru, *Applied Catalysis B: Environmental* 202, 21(2017).
- [10] M Amir, M Sertkol, A Baykal, H Sözeri, *J. Supercond. Nov. Magn.*, 28, 2447 (2015).
- [11] S Dasgupta, B Das, Q Li, D Wang, TT Baby, S Indris, *Adv. Funct. Mater.* 26,7507(2016).
- [12] H Guo, A Marchilok, KJ Takeuchi, ES Takeuchi, *Advanced materials interfaces*, 6(22), 1901218 (2019).
- [13] Y Li, X Xu, C Ding, N Chen, H Ding, A Lu, *Chem. Geol.* 504, 276 (2019).

- [14] M Nawaz, A Shahzad, K Tahir, J Kim, M Moztahida, J Jang, Chem. Eng. J. 382, 123053 (2020).
- [15] KK Kefeni, BB Mamba, TAM Msagati, Sep. Purif. Technol. 188, 399 (2017).
- [16] MB Gawande, A Goswami, FX Felpin, T Asefa, X Huang, R Silva, X Zou, R Zboril, RS Varma, Chem. Rev., 3722-3811 (2016).
- [17] J Du, J Bao, X Fu, C Lu, S Hoon, *Appl. Catal. B: Environ.*, 184, 132 (2016).
- [18] J Deng, S Feng, X Ma, C Tan, H Wang, S Zhou, Sep. Purif. Technol. 167, 181 (2016).
- [19] Y Zhang, L Liu, Q Chen, Y He, MKH Leung, Chem. Eng. J. 378, 122148 (2019).
- [20] G Zeng, N Shi, M Hess, X Chen, W Cheng, T Fan, ACS Nano 9, 4227 (2015).
- [21] J Mohapatra, M Xing, JP Liu, Materials, 12, 26 (2019).
- [22] A Rostami, B Atashkar, H Gholami, Catal. Commun., 37, 69 (2013).
- [23] M Nadimi, A Ziarati Saravani, MA Aroon, E Pirbazari, Mater. Chem. Phys., 225, 464 (2019).
- [24] Y Zhao, B Cao, Z Lin, X Su, Environ. Pollut., 254, 112961 (2019).
- [25] K Zhu, C Jin, C Zhao, R Hu, Z Klencsár, Chem. Eng. J., 359, 1537 (2019).
- [26] E Casbeer, VK Sharma, X Li, Sep. Purif. Technol. 87, 1 (2012).
- [27] B Ren, Y Huang, C Han, MN Nadagouda, DD Dionysiou, Am. Chem. Soc., 79–112 (2016).
- [28] TR Tatarchuk, M Bououdina, JJ Vijaya, LJ Kennedy, J. Alloys Compd., 694, 777 (2017).
- [29] N Chaibakhsh, Z Moradi-Shoeili, Mater. Sci. Eng., C 99, 1424 (2019).
- [30] MV L´opez-Ram´on, MA´Alvarez, C Moreno-Castilla, MA Fontecha-C´amara, A Yebra-Rodríguez ´, E Bail´on-García, J. Colloid Interface Sci., 511, 193 (2018).
- [31] A Evdou, V Zaspalis, L Nalbandian, Fuel, 165, 367 (2016).

- [32] PA Vinosha, B Xavier, S Krishnan, S Das, J Mater. Res. Bull.,101,190 (2018).
- [33] Y Sun, Y Diao, H Wang, G Chen, M Zhang, M Guo, Ceram. Int., 43,16474 (2017).
- [34] S Stankic, S Suman, F Haque, J Vidic, J. Nanobiotechnol.,14,1 (2016).
- [35] T Prabhakaran, RV Mangalaraja, JC Denardin, Alloys and Comp. J., 716, 171 (2017).
- [36] TL Ajeesha, A. Ashwini, M George, A Manikandan, J Arul Maryc, Y Slimani, Physica B: Physics of Condensed Matter, 606, 412660 (2021).
- [37] R Safi, A Ghasemi, R Shoja-Razavi, E Ghasemi, T Sodaee, Ceram. Int., 42, 6375–82 (2016).
- [38] M Nawaz, MA Almessiere, SA Almofty, CD Gungunes, Y Slimani, A Baykal, J. Photochem. Photobiol. B Biol.,196,111506 (2019).
- [39] Y Sun, Y Diao, H Wang, G Chen, M Zhang, M Guo, Ceram. Int., 43,16474 (2017).
- [40] G Wang, D Zhao, F Kou, Q Ouyang, J Chen, Z Fang, Chem. Eng. J., 351,747 (2018).
- [41] V Marutha pandian, M Mathan kumar, B Subramanian, S Muralidharan, ACS Appl. Mater. Interfaces, 9,13132 (2017).
- [42] IJC Lynda, M Durka, A Dinesh, A Manikandan, SK Jaganathan, A Baykal, J. Supercond. Nov. Magn., 31,3637 (2018).
- [43] G Fan, Z Gu, L Yang, F Li, Chem. Eng. J.,155,534 (2009).
- [44] R Dom, AS Chary, R Subasri, NY Hebalkar, PH Borse, Int. J. Energy Res., 39, 1378 (2015).
- [45] X Han, H Zhang, T Chen, M Zhang, M Guo, J. Mol. Liq., 272, 43(2018).
- [46] D Peeters, DH Taffa, MM Kerrigan, A Ney, N J'ons, D Rogalla, ACS Sustain. Chem. Eng., 5, 2917 (2017).
- [47] C Zhang, S Bhoiyate, C Zhao, PK Kahol, N Kostoglou, C Mitterer, Catalysts, 9,176 (2019).

- [48] AG Hufnagel, K Peters, A Müller, C Scheu, D Fattakhova-Rohlfing, T Bein, *Adv. Funct. Mater.*, 26, 4435 (2016).
- [49] B He, J Wang, J Liu, Y Li, Q Huang, Y Hou, *Adv. Energy Mater.*, 1904262, 1 (2020).
- [50] PK Dikshit, J Kumar, AK Das, S Sadhu, S Sharma, S Singh, PK Gupta, BS Kim, *catalysis*, 11(8), 902 (2021).
- [51] T Parandhaman, N Pentela, B Ramalingam, D Samanta, SK Das, *ACS Sustain. Chem. Eng.*, 5, 489 (2017).
- [52] K Kombaiah, JJ Vijaya, LJ Kennedy, M Bououdina, *Ceram. Int.*, 42, 2741 (2016).
- [53] M Amiri, M Salavati-Niasari, A Pardakhty, M Ahmadi, A. Akbari, *Sci. Eng. C*, 76,1085 (2017).
- [54] M Amiri, A Pardakhti, M Ahmadi-Zeidabadi, A. Akbari, M Salavati-Niasari, *Colloids Surf. B: Biointerfaces*, 172, 244 (2018).
- [55] MM Naik, HSB Naik, G Nagaraju, M Vinuth, HR Naika, K Vinu, *Microchem. J.*, 146, 1227 (2019).
- [56] M Amiri, Akbari, M Ahmadi, A Pardakhti, M Salavati-Niasari, *J. Mol. Liq.*, 249,1151 (2018).
- [57] BS Surendra, *J. Sci.: Adv. Mater. Dev.*, 3, 44 (2018).
- [58] MN Moura, RV Barrada, JR Almeida, TFM Moreira, MA Schettino, JCC Freitas, *Chemosphere*, 2017;182, 339 (2017).
- [59] VS Morais, RV Barrada, MN Moura, JR Almeida, TFM Moreira, GR Gonçalves, *J. Environ. Eng.*, 8,103716 (2020).
- [60] P Samoila, C Cojocar, L Sacarescu, PP Dorneanu, AA Domocos, A Rotaru, *Appl. Catal. B Environ.*, 202, 21 (2017).
- [61] Md Amir, M Sertkol, A Baykal, H Sözeri, *J. Supercond. Nov. Magn.*, 28, 2447 (2015).

- [62] M Sundararajan, L John Kennedy, P Nithya, J Judith Vijaya, M Bououdina, *J. Phys. Chem. Solids*, 108, 61 (2017).
- [63] X Li, X Sun, J Wang, Q Liu, *J. Alloys Compd.*, 582, 398 (2014).
- [64] D Cao, X Wang, L Pan, H Li, P Jing, *J. Mater. Chem.*, C 4, 951 (2016).
- [65] J Wang, Y Wang, X Xv, Y Chen, X Yang, J Zhou, et al., *Dalton Trans.*, 48,11934 (2019).
- [66] P Liu, H He, G Wei, X Liang, F Qi, *Appl. Catal. B Environ.*, 182, 476 (2016).
- [67] S Ikram, M Alzaid, K Mahmood, N Amin, SA Haider, *J. Supercond. Nov. Magn.*, <https://doi.org/10.1007/s10948-020-05723-8> (2020).
- [68] GB Todkar, Kunale, RN Kamble, M Batoo Khalid, MF Ijaz, A Imran, *J. PhysD. Appl. Phys.*, 54, 294001 (2021).
- [69] M Hadi, KM Batoo, A Chauhan, O Aldossary, R Verma, *Magnetochemistry*, 7, 5 (2021).
- [70] SE Shirsath, RH Kadam, KM Batoo, D Wang, S Li, *J. Phys. D. Appl. Phys.*, 54, 024001 (2021).
- [71] X Xu, AK Azad, JTS Irvine, *Catal. Today*, 199, 22 (2013).
- [72] WRP Barros, JR Steter, MRV Lanza, AC Tavares (2016) *Appl. Catal. B Environ.*, 180, 434.
- [73] R Sharma, S Bansal, S Singhal, *RSC Adv.*, 5, 6006 (2015).
- [74] TR Tatarchuk, M Bououdina, ND Paliychuk, IP Yaremiy, VV Moklyak, *J. Alloys Compd.* 694,777 (2017).
- [75] J Zhang, X Shang, H Ren, J Chi, H Fu, B Dong, *Adv. Mater.*, 31,1905107 (2019).
- [76] Q Wang, K Domen, *Chem. Rev.* 120, 919 (2020).
- [77] Q Yue, C Liu, Y Wan, X Wu, X Zhang, P Du, *J. Catal.*, 358,1(2018).
- [78] H Yang, Y Liu, S Luo, Z Zhao, X Wang, Y Luo, *ACS Catal.*, 7, 5557(2017).

- [79] Y Wang, J Cai, M Wu, J Chen, W Zhao, Y Tian, *Appl. Catal. B Environ*, 239, 398–407 (2018).
- [80] H Zhang, C Li, L Lyu, C Hu, *Appl. Catal., B* 270, 118874 (2020).
- [81] J Sun, N Guo, Z Shao, K Huang, Y Li, F He, *Adv. Energy Mater*, 8,1800980 (2018).
- [82] L Wu, Y Yu, Q Zhang, J Hong, J Wang, Y She, *Appl. Surf. Sci.*, 480, 717(2019).
- [83] YL Huang, WB Fan, YH Hou, KX Guo, YF Ouyang, ZW Liu, *J. Magn. Magn. Mater*, 429, 263 (2017).
- [84] CVVM Gopi, R Vinodh, S Sambasivam, IM Obaidat, S Singh, HJ Kim, *Chem. Eng. J.*, 381, 122640 (2020)
- [85] H Salazar-Tamayo, KEG Tellez, CAB Meneses, *Mater. Res.*, 22, 20190298 (2019).
- [86] L Zhou, L Ji, P Ma, Y Shao, *J. Hazard. Mater.*, 265, 104 (2014).
- [87] AA Farghali, M Bahgat, WMA Elrouby, MH Khedr, *J. Nanostructure in Chem.*, 3, 1(2013).
- [88] P Xu, G Zeng, D Huang, M Yan, M Chen, C Lai, *J. Taiwan Inst. Chem. Eng.*, 71,165 (2017).
- [89] X Wang, A Wang, J Ma, *J. Hazard. Mater.*, 336, 81 (2017).
- [90] T Li, Y Lv, J Su, Y Wang, Q Yang, Y Zhang, *Adv. Sci.*, 4, 1700226 (2017).
- [91] L Lu, Q Hao, W Lei, X Xia, P Liu, D Sun, *Small*,11, 5833 (2015).
- [92] H Hajiyani, R Pentcheva, *ACS Catal.*, 8,11773 (2018).
- [93] U Kurtan, A Baykal, *Mater. Res. Bull.*, 2014; 60, 79 (2014).
- [94] U Kurtan, A Baykal, H Sözeri, *J. Inorg. Organomet. Polym. Mater.*, 25, 921(2015).
- [95] L Qin, Z Xu, Y Zheng, C Li, J Mao, G Zhang, *Adv. Func. Mat*, 30, 1910257(2020).
- [96] JJ Pignatello, E Oliveros, A MacKay, *Crit. Rev. Environ. Sci. Technol.*, 36, 1(2006).

- [97] M Fukushima, K Tatsumi, K Morimoto, *Environ. Sci. Technol.*, 34, 2006 (2000).
- [98] Z Liu, S Yang, Y Yuan, J Xu, Y Zhu, J Li, *J. Hazard. Mater.*, 324, 583 (2017).
- [99] X Dong, B Ren, Z Sun, C Li, X Zhang, M Kong, *Appl. Catal. B Environ*, 253, 206 (2019).
- [100] R Li, M Cai, Z Xie, Q Zhang, Y Zeng, H Liu, *Appl. Catal. B Environ.*, 244, 974 (2019).
- [101] BM Jun, SS Elanchezhian, Y Yoon, D Wang, S Kim, S Muthu Prabhu, *Chem. Eng. J.*, 393, 124733 (2020).
- [102] Z Wang, C Lai, L Qin, Y Fu, J He, D Huang, *Chem. Eng. J.*, 392, 124851 (2020).
- [103] JJ Rodriguez, M Munoz, ZM De Pedro, JA Casas, *Appl. Catal. B Environ.*, 176, 249 (2015).
- [104] P Baldrian, MJ Benes, P Stopka, M Hruby, *Appl. Catal. B Environ.*, 66, 258–64 (2006).
- [105] C Cai, Z Zhang, J Liu, N Shan, H Zhang, DD Dionysiou, *Appl. Catal. B Environ.*, 18, 456 (2016).
- [106] Y Huang, C Han, Y Liu, MN Nadagouda, L Machala, KE O'Shea, *Appl. Catal. B Environ.*, 221, 380 (2018).
- [107] S Yang, X Qiu, P Jin, M Dzakpasu, XC Wang, Q Zhang, *Chem. Eng. J.*, 353, 329 (2018).
- [108] S Yang, X Guo, Z Wang, M Dzakpasu, X Dai, D Ding, *Chem. Eng. J.*, 359, 552 (2019).
- [109] Y Lei, X Lin, H Liao, *Sep. Purif. Technol.*, 220 (2018).
- [110] S Samakchi, N Chaibakhsh, Z Moradi-Shoeili, *J. Photochem. Photobiol. A Chem.*, 367, 420 (2018).
- [111] CM Park, J Heo, D Wang, C Su, Y Yoon, *Appl. Catal. B Environ.*, 225, 91 (2018).
- [112] SHS Chan, TY Wu, JC Juan, CY The, *J. Chem. Technol. Biotechnol.*, 86, 1130 (2011).
- [113] SJA Moniz, SA Shevlin, DJ Martin, ZX Guo, J Tang, *Energy Environ. Sci.*, 8, 731 (2015).
- [114] M Ge, Q Li, C Cao, J Huang, S Li, S Zhang, *Adv. Sci.*, 2017;4,1 (2017).

- [115]WHM Abdelraheem, MK Patil, MN Nadagouda, Appl. Catal. B Environ., 241, 598 (2019).
- [116]E Skliri, J Miao, J Xie, G Liu, T Salim, B Liu, Appl. Catal. B Environ, 227, 330 (2018).
- [117]A Al-Anazi, WH Abdelraheem, C Han, MN Nadagouda, L Sygellou, MK Arfanis, Appl. Catal. B Environ., 221, 266 (2018).
- [118]S Yang, X Qiu, P Jin, M Dzakpasu, XC Wang, Q Zhang et al., Chem. Eng. J., 353, 329(2018).
- [119]M Kamranifar, A Allahresani, A Naghizadeh, J. Hazard. Mater., 366, 545 (2019).
- [120]R Cheng, X Fan, M Wang, M Li, J Tian, L Zhang, RSC Adv., 6,18990 (2016).
- [121]J Zeng, T Song, M Lv, T Wang, H Zeng, RSC Adv., 6, 54964 (2016).
- [122]J Low, B Cheng, J Yu, Appl. Surf. Sci., 392, 658 (2017).
- [123]B Gholamkhas, H Mametsuka, K Koike, T Tanabe, M Furue, Inorg. Chem., 44, 2326 (2005).
- [124]S Naval'on, A Dhakshina moorthy, Chem Sus Chem, 6, 562 (2013).
- [125]J Guo, K Wang, X Wang, Catalysis Science and Technology, 7, 6013 (2017).
- [126]S Vadivel, D Maruthamani, A Habibi-Yangjeh, B Paul, SS Dhar, K Selvam, J. Colloid Interface Sci., 480, 126 (2016).
- [127]T Vijayaraghavan, SP Suriyaraj, R Selvakumar, R Venkateswaran, A Ashok, Materials Science and Engineering B: Solid-State Materials for Advanced Technology, 210, 43 (2016).
- [128]SK Rashmi, HS Bhojya Naik, H Jayadevappa, R Viswanath, SB Patil, M Madhukara Naik, Mat. Sci. and Eng. B: Solid-State Materials for Adv. Technol., 225, 86 (2017).
- [129]EF Attia, AH Zaki, SI El-Dek, AA Farghali, J. Mol. Liq., 231, 589 (2017).
- [130]S Fan, X Li, L Zeng, M Zhang, Z Yin, T Lian, ACS Appl. Mater. Interfaces,10(42), 35919 (2018).

- [131]X Ge, A Sumboja, D Wu, B Li, FWT Goh, ACS Catal., 5, 4643 (2015).
- [132]R Karunakaran, C Coghlan, T Tung, J. Chem., 41, 15180 (2017).
- [133]Y Xiong, Y Yang, X Feng, FJ Disalvo, HD Abruña, J. Am. Chem. Soc.,141, 4412 (2019).
- [134]Y Zhou, Y Du, S Xi, ZJ Xu, Electrocatalysis, 9, 287 (2018).
- [135]X Wang, T Ouyang, L Wang, J Zhong, T Ma, Z Liu, Angew. Chem., 131, 13425 (2019).
- [136]X Zhao, Y Fu, J Wang, Y Xu, JH Tian, R Yang, Electrochim. Acta, 201, 172 (2016).
- [137]T Binh, CP Huang, R Doong, Sci. Total Environ., 646,745 (2019).
- [138]L Lu, X Jiao, J Fan, W Lei, Y Ouyang, X Xia, Electrochim. Acta, 295, 461 (2019).
- [139]X Gao, J Liu, Y Sun, X Wang, Z Geng, F Shi, Inorganic Chemistry Frontiers, 6, 3295 (2019).
- [140]Y Huang, W Yang, Y Yu, S Hao, J Electroanal. Chem., 840, 409 (2019).
- [141]Y Guo, N Zhang, X Wang, Q Qian, S Zhang, Z Li, J. Mater. Chem. A, 5, 7571 (2017).
- [142]TK Sahu, AK Shah, G Gogoi, AS Patra, MS Ansari, M Qureshi, Chem. Commun., 54,10483 (2018).
- [143]J Wang, Y Wang, X Xu, Y Chen, X Yang, J Zhou, Dalton Trans., 48, 11934 (2019).
- [144]N Guijarro, P Bornoz, M Prévot, X Yu, X Zhu, M Johnson, et al., Sustainable Energy and Fuels, 2,103 (2018).
- [145]M Horie, H Kato, H Iwahashi, Arch. Toxicol., 87, 771 (2013).
- [146]F Ahmad, X Liu, Y Zhou, H Yao, Aquat. Toxicol.,166, 21 (2015).
- [147]R Colognato, A Bonelli, D Bonacchi, G Baldi, R Colognato, A Bonelli, et al., Nanotoxicology, 1, 301 (2007).
- [148]L Horev-azaria, G Baldi, D Beno, D Bonacchi, U Golla-schindler, JC Kirkpatrick, et al., Particle and Fibre Toxicol.,10, 1 (2013).

- [149]P Zan, C Yang, H Sun, L Zhao, Z Lv, Y He., Colloids Surf. B: Bio interfaces,145, 208(2016).
- [150]F Coppola, DS Tavares, B Henriques, R Monteiro, T Trindade, E Figueira, et al., Sci. Total Environ., 723, 137798 (2020).
- [151]S Mirzaee, J Aust. Ceram. Soc., 56,1021 (2020).
- [152]P Anastas, N Eghbali, Chem. Soc. Rev., 39, 301 (2010).
- [153]A Al-anazi, WH Abdelraheem, K Scheckel, MN Nadagouda, KO Shea, DD Dionysiou, Applied Catalysis B: Environmental, 275, 119098 (2020).

HOW TO CITE THIS ARTICLE

Vidya Singh. "An overview on recent trends of spinel ferrites (MFe_2O_4 : $M= Fe^{2+}$, Co^{2+} , Mn^{2+} , Ni^{2+} , Zn^{2+}) synthesis and catalytic applications", International Journal of New Chemistry, 2024; 12(3), 283-317. doi: 10.22034/ijnc.2024.2032437.1398